

Article

Electromagnetic Property Modulation of Flaky Ferromagnetic 304 Stainless-Steel Powders for Microwave Absorption at Elevated Temperatures

Bolin Yang ¹, Yifan Xu ², Zhihong Chen ^{3,*}, Hang Yang ¹, Yuchen Hu ³, Haoqin Wu ⁴, Mingfeng Xing ¹, Jianguo Guan ² and Wei Li ^{5,*}

¹ School of Materials Science and Engineering, Wuhan University of Technology, Wuhan 430070, China

² School of Materials and Microelectronics, Wuhan University of Technology, Wuhan 430070, China

³ School of Science, Wuhan University of Technology, Wuhan 430070, China

⁴ Leicester International Institute, Dalian University of Technology, Dalian 116024, China

⁵ State Key Laboratory of Advanced Technology for Materials Synthesis and Processing, Wuhan University of Technology, Wuhan 430070, China

* Correspondence: z_chen@whut.edu.cn (Z.C.); wellee@whut.edu.cn (W.L.)

Abstract: Soft magnetic metallic absorbents suffer from severe oxidation, reduction in permeability and deterioration in microwave absorption when exposed to high temperatures. In this study, we prepared flaky 304 stainless-steel powders as new microwave absorbents via deformation-induced ferromagnetism. The 304 stainless-steel powders showed significant increases in saturation magnetization (M_s) from 1.03 to 82.46 emu/g when their shape was changed from spheroids to flakes; the M_s further increased to 92.29 emu/g after heat treatment at 500 °C in air. The permeability of 304 alloy powders also showed an obvious increase after ball milling and remained roughly stable after heat treatment at 500 °C in air. Moreover, the permittivity exhibited a sharp decrease after heat treatment, enabling the improvement of impedance matching and microwave absorption. After heat treatment at 500 °C in air for 100 h, the simulated reflection loss of 304 stainless-steel powders with wax still showed attractive levels, giving a minimum value of -22 dB and remaining below -6 dB over 8.5–16.5 GHz at a thickness of 2 mm. Our work can help to include paramagnetic alloy systems as new microwave absorbents for working in harsh environments.

Keywords: 304 austenitic stainless-steel powders; microwave absorption; ball milling; magnetic loss; thermal stability



Citation: Yang, B.; Xu, Y.; Chen, Z.; Yang, H.; Hu, Y.; Wu, H.; Xing, M.; Guan, J.; Li, W. Electromagnetic Property Modulation of Flaky Ferromagnetic 304 Stainless-Steel Powders for Microwave Absorption at Elevated Temperatures. *Magnetochemistry* **2023**, *9*, 208. <https://doi.org/10.3390/magnetochemistry9090208>

Academic Editor:
Krzysztof Chwastek

Received: 4 August 2023
Revised: 27 August 2023
Accepted: 29 August 2023
Published: 5 September 2023



Copyright: © 2023 by the authors. Licensee MDPI, Basel, Switzerland. This article is an open access article distributed under the terms and conditions of the Creative Commons Attribution (CC BY) license (<https://creativecommons.org/licenses/by/4.0/>).

1. Introduction

Heat-resistant absorbents are key functional components of microwave-absorbing materials working at elevated temperatures for applications in electromagnetic protection and stealth for military/civilian equipment [1–3]. At present, the developed heat-resistant absorbents, such as carbon-based materials [4], ceramics [5–7] and metal oxides [8], mainly attenuate microwaves via dielectric loss. These materials generally show excellent oxidation resistance and stable phase structure at high temperatures, while their single loss mechanism and difficulty in regulating dielectric dispersion give rise to disadvantages such as narrow absorption bandwidths and great thicknesses [9,10]. In contrast, magnetic metallic absorbents, such as iron, cobalt, nickel and their alloys, demonstrate both magnetic and dielectric loss mechanisms in response to microwaves [11,12]. Magnetic metallic absorbents have shown advantages for obtaining thin microwave-absorbing coatings with wide bandwidth. Also, by adjusting composition, the magnetic resonance frequency can be purposely controlled or designed [13]. In addition, higher Curie temperatures (such as 770 °C for Fe and 1130 °C for Co) [14] indicate the potential of magnetic alloys as heat-resistant absorbents [15–17]. However, due to the active chemical properties of magnetic

metallic absorbents, severe oxidation causes performance deterioration at elevated temperatures [18]. Therefore, it is of great significance to develop new magnetic metallic absorbents with excellent and stable performance at elevated temperatures.

To improve the oxidation resistance of magnetic metallic absorbents, surface coating has been employed as the main method to reduce or avoid oxygen–metal interface reactions [19]. Organics, inorganic compounds, metals and alloys have been reported as coating materials for magnetic metallic absorbents to isolate the contact between absorbents and oxygen [20,21]. Organic coating materials such as polyaniline are compatible with polymer matrices, and their redox properties can induce the stable passivation of Fe [21,22]. Non-magnetic inorganic compounds such as SiO₂ [23,24] and Al₂O₃ [25] can adjust impedance matching while forming a dense protective layer or multilevel composite shell. The coating of magnetic elements such as Co [26] and Ni [27] can reduce the influence of coating materials on the permeability of absorbents. However, the decomposition or oxidation of coating materials, as well as the difficulties in preparing dense coatings with pores smaller than oxygen molecules [28–30], hinders the long-term service of magnetic metallic absorbents at elevated temperatures.

Besides surface coating, alloying is another strategy used to obtain heat-resistant microwave absorbents. Doping Al, Cr, Si or other alloying elements that have high affinities for oxygen and high diffusion rates into the alloy can form a dense oxidation layer on the external surface of Fe and hence inhibit further oxygen diffusion/metal oxidation [31–33]. Nevertheless, it is difficult to achieve excellent anti-oxidation ability with a single element, and thus doping with multiple elements is required. Among alloys of Fe with other elements, the production of various stainless steels is the best example [34]. Ferrite stainless-steel powders have certain magnetic properties in the microwave band, which makes them a kind of microwave absorbent with potential applications. Yang et al. [35] studied the microwave-absorption performance of ferrite stainless-steel powders such as 409L and 410L and found that their permeability was generally low and their microwave absorption was not strong. Meanwhile, this kind of stainless steel has poor plasticity [36]; hence, it is difficult to further improve the permeability by flaking particles. Compared with ferritic stainless steel, austenitic stainless steels such as 304 and 316L have better corrosion/oxidation resistance and plasticity due to the extra content of Ni [37], but their crystal structures are paramagnetic, face-centered and cubic [38], which limits their applications in microwave absorption.

It is worth noting that 304 austenitic stainless steel has a relatively low stacking fault energy, and its metastable austenitic structure is prone to strain-induced martensite transformation [39]. During plastic deformation, 304 stainless-steel powder tends to exhibit an obvious increase in saturation magnetization (M_s) [40,41] and refinement of grains to the nanometer level [42], which makes it possible to be used as a microwave absorbent. However, although austenitic stainless steels such as 304 or 316 L exhibit martensitic phase transformation, the microwave absorption introduced by this effect is still unknown, and the electromagnetic stability of flaky stainless-steel powders at high temperatures needs to be investigated.

In this study, we induced the ferromagnetic transformation of 304 austenitic stainless-steel powders with increased shape anisotropy via ball milling. The microstructure, magnetostatic properties and permeability dispersion of the 304 powders during phase transition were studied. Subsequent heat treatment was carried out to improve the impedance matching and test the heat resistance of resultant absorbents. Results showed that the M_s of 304 stainless-steel powders increased from 1.03 to 92.29 emu/g after thermal deformation treatment, under which microwave absorption performance was significantly enhanced and remained stable at 500 °C. This work can provide new selections for microwave-absorbing materials working at elevated temperatures.

2. Materials and Methods

A 304 stainless-steel powder with 18.75 wt.% of Cr, 10.85 wt.% of Ni, 1.54 wt.% of Mo, 0.39 wt.% of Mn, 1.46 wt.% of Si and residual Fe was prepared by gas atomization by Guangzhou Metal Metallurgical Materials Company, Guangzhou, China. To enhance the effect of deformation-induced martensitic transformation, the powder was subjected to vacuum heat treatment at 800 °C to obtain a pure austenitic phase before ball milling.

The 304 stainless-steel powders were subjected to high-energy ball milling to induce plastic deformation and shape anisotropy. The process involved adding 20 g of raw powders and 400 g of zirconia balls to a ball-mill tank, along with 13 mL of cyclohexane as the process control agent. The milling rate was set as 300 r/min, with a ball-to-powder weight ratio of 20:1. The powders obtained after milling for different durations were separated from the milling balls using a sieve and collected by a filter. The collected powders were then dried at 60 °C for 3 h. To study the heat resistance of 304 stainless-steel powders, a clean crucible was used, and the powders were placed inside. The samples were heated at a rate of 10 °C/min to the predetermined temperature. After heat treatment, the powders were cooled naturally to room temperature.

In order to measure the electromagnetic parameters, a mixture of 304 stainless-steel powder and paraffin wax was prepared with volume fraction of 28% for the 304 stainless-steel powder. This mixture was then pressed into a coaxial ring shape with an outer diameter of 7 mm, inner diameter of 3 mm, and thickness of 2–3 mm. A pressure of 10 MPa was used to prepare the coaxial ring samples. The complex permittivity and permeability were measured using an Agilent E5071C (Palo Alto, CA, USA) vector network analyzer. The morphology of the 304 stainless-steel powders was analyzed by scanning electron microscopy (SEM, Hitachi S4800, Tokyo, Japan). The crystal structure of the powders was studied by X-ray diffraction (XRD, Karlsruhe, Germany). Additionally, the static magnetic properties of the powders were measured using a Lakeshore 7404 (Chicago, IL, USA) vibrating sample magnetometer (VSM). The VSM tests were conducted at least three times to ensure accuracy.

3. Results and Discussion

To study the evolution of microstructure and crystal structure in 304 stainless-steel powders during ball milling, powders with different ball-milling times were characterized by XRD and SEM. The shape anisotropy changes during ball milling are shown in Figure 1a–c. Figure 1a shows that most of raw powders were spherical particles with a particle size less than 70 μm, and a small amount of irregular particles can be observed due to the coalescence of droplets during aerosol atomization [43]. With the extension of ball-milling time, the 304 stainless-steel powders changed from spherical to flaky under the action of the impact force generated by the collision of milling balls and the shear force generated by the rotation of milling balls [44]. After ball milling for 6 h, the 304 stainless-steel powders were highly flaky, and the particle width also increased (Figure 1b). However, when the milling time was further prolonged, the energy transferred to the powders by milling balls led to the initiation and development of cracks inside the particles, and the surface smoothness of the particles was reduced. After reaching the plastic deformation limit, the powders broke into small pieces (see Figure 1c), and the particle size decreased significantly. After ball milling for 30 h or even 40 h, the particle size was stable (see Figures S1 and S2 in Supplementary Information), indicating that the particle size reduction and agglomeration reached a balance at 20 h of ball milling [45].

The XRD pattern in Figure 1d–f shows the phase change in 304 stainless-steel powders during ball milling. The results showed that the raw 304 alloy powders changed into a single austenite phase (γ -Fe) after vacuum annealing at 800 °C (as shown in Figure 1d). During ball milling for up to 6 h, the content of the martensite phase (α' -Fe) in the powders increased continuously, while the characteristic peak of the γ phase decreased gradually. The crystal structure was relatively stable during ball milling from 6 h to 12 h, and there was no significant increase in α' phase content. After reaching the limit of particle plas-

tic deformation, the particles broke due to strain hardening [46]. After ball milling for 20 h, the alloy powders exhibited mainly α' phase with a small amount of γ phase, which may be due to the small grain size or the residual stress generated during ball milling to stabilize the martensite phase [42]. The whole ball-milling process caused the decay of the γ phase and the development/growth of the α' phase. Previous studies showed [40] that the ε phase of 304 stainless-steel powders grew initially and then decayed during deformation-induced martensitic transformation; however, its content may be lower than the detection limit of X-ray diffraction. In this work, at the initial stage of ball milling, the diffraction peak in the X-ray spectrum was obviously widened, and the subsequent process of ball milling was almost constant, indicating that the grains were rapidly refined at the initial stage and remained stable after that; this was due to the high-density dislocation generated by severe mechanical processing in high-energy ball milling [47].

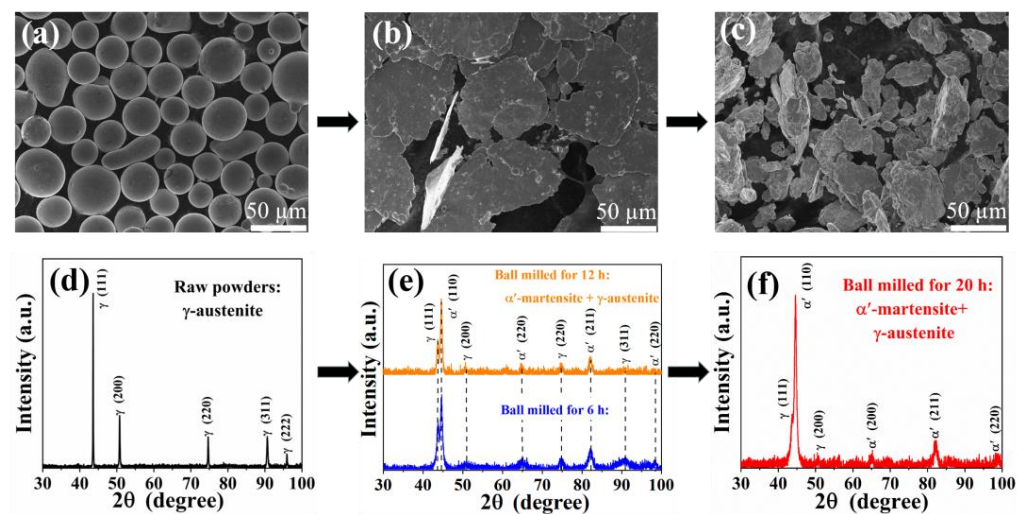


Figure 1. (a–c) SEM images of (a) raw 304 stainless-steel powders and those after ball milling for (b) 6 h and (c) 20 h; (d–f) XRD pattern of (d) raw 304 stainless-steel powders and those after ball milling for (e) 6 h, 12 h and (f) 20 h.

According to the XRD pattern and SEM images, the 304 alloy powders reached the flaking limit after 6–12 h of ball milling, and the martensite phase transition was nearly completed at 20 h of ball milling. However, the particles also broke seriously during long-term milling, which caused the destruction of crystal structure [48]. The degree of the $\gamma \rightarrow \alpha'$ phase transition mainly depended on the chemical composition of the steel. According to the relationship between the stacking fault energy (SFE) and the contents of Cr, Ni, Mn and Mo reported by Juho [49], the SFE can be expressed by

$$\text{SFE} = -53 + 6.2\omega(\text{Ni}) + 0.7\omega(\text{Cr}) + 3.2\omega(\text{Mn}) + 9.3\omega(\text{Mo}) \quad (1)$$

where $\omega(\text{Ni})$, $\omega(\text{Cr})$, $\omega(\text{Mn})$ and $\omega(\text{Mo})$ are contents of Cr, Ni, Mn and Mo, respectively. It could be seen that when the content of these elements decreased, the SFE of stainless steel continuously decreased. The generation of more stacking faults provided more martensitic nucleation sites, thus significantly increasing the tendency of deformation-induced martensitic transformation [50]. However, the morphology and microstructure evolution of powders during ball milling obviously depended on ball-milling parameters such as milling rate and time, ball-to-powder weight ratio and process control agents [48]. High Ni content would stabilize the austenite phase [51], which may be the cause of incomplete phase transition in our experiment. A higher milling rate and ball-to-powder weight ratio may coordinate the progress of flaking and martensitic phase transition [52].

The magnetic properties of 304 stainless-steel powders were studied. Figure 2a shows the hysteresis loop of 304 stainless-steel powders at different milling times. It can be

seen that the M_s of raw powders was negligible, with a value of only 1.05 ± 0.01 emu/g, confirming the single austenitic paramagnetic structure. It was well known that the α' phase in martensite was proven to be the only ferromagnetic phase; thus, the change in M_s could reflect a change in the volume fraction of α' martensite. The M_s of the alloy powders increased gradually during ball milling and reached 82.46 ± 0.97 emu/g after ball milling for 20 h. Figure 2b shows the magnified hysteresis loops when the magnetic field intensity was close to 0. It can be seen that the slope and initial permeability (μ_i) of powders reached the highest value after ball milling for 6 h, corresponding to the maximum width-to-thickness ratio. With the extension of milling time, the width-to-thickness ratio and initial permeability of particles decreased. Figure 2c shows the variation trends in M_s and coercivity (H_c) with ball-milling time. The result indicates that the transformation rate of the martensitic phase gradually decreased, since the probability of capturing the powders in the austenitic phase tends to decrease with the extension of ball-milling time [53]. At the same time, in the VSM test of powders after ball milling for 12 h, the standard deviation of parallel tests was relatively large. This result may be due to the increase in grain defects caused by long-term ball milling, leading to a decrease in measured magnetization [54]. After ball milling for 20 h, grain fragmentation resulted in the deterioration of H_c and μ_i , while M_s increased due to the further formation of martensite phase.

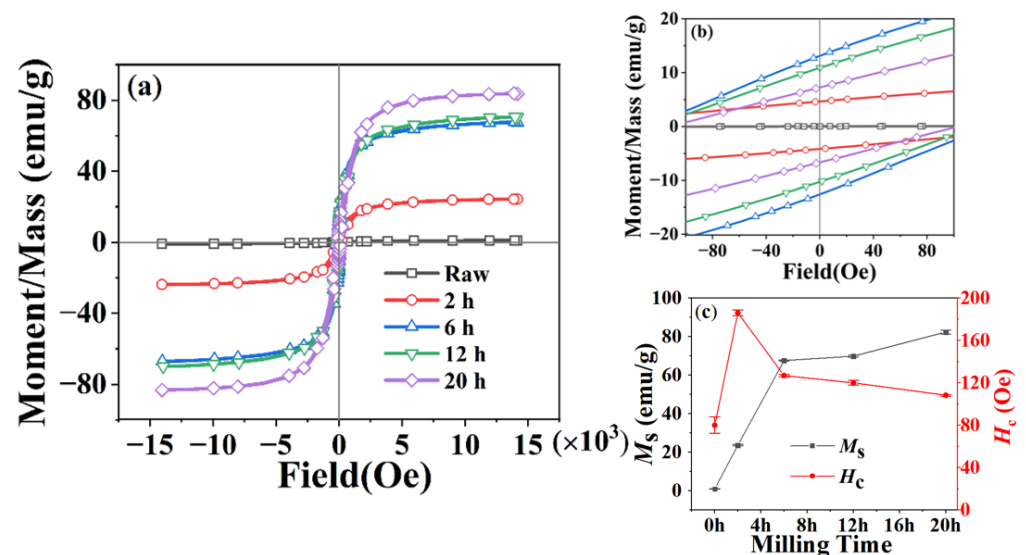


Figure 2. Magnetic properties of 304 stainless-steel powders after ball milling for different times: (a) hysteresis loop, (b) local hysteresis loop at low magnetic field, (c) changes in M_s and H_c with ball-milling time.

The H_c of the 304 alloy powders surged after ball milling for 2 h. With the extension of ball-milling time, H_c gradually decreased, showing an opposite change tendency to that of M_s . It has been reported that H_c is more sensitive to material microstructure than M_s [55]. The internal stress in powders introduced by the collision and rotation of balls caused lattice distortion in the austenitic phase, resulting in a sharp increase in H_c in the early stage of ball milling. In the subsequent ball-milling process, the austenite phase changed into martensite under the action of stress, along with a decrease in atomic arrangement density and hence the release of lattice distortion energy [56]. Meanwhile, the increase in martensite content strengthened the ferromagnetic exchange between adjacent domains [57], resulting in a decrease in H_c .

The complex permeability and permittivity of 304 stainless-steel powders at different ball-milling times were further studied. Figure 3a,b shows the frequency-dependent characteristics of the complex permittivity ($\epsilon_r = \epsilon' - i\epsilon''$) of 304 stainless-steel powders in wax over 1.0–18.0 GHz. At a ball-milling time of less than 6 h, the permittivity increased gradually with the increase in milling time; ϵ' increased from 5.70 to 137.23 and ϵ'' increased

from 0.20 to 144.28 at 1 GHz. The increase in permittivity was due to the increase in space-charge polarization and interparticle eddy current. In the first 6 h of ball milling, particles underwent plastic deformation and exhibited greater surface area/grain defects, which contributed to an enhancement in the space-charge polarization of particles in an external alternating electric field [58]. Also, flaky particles were more likely to overlap each other to form a conducting network and hence increase the conductivity σ and eddy current. According to the free electron theory [59],

$$\varepsilon'' = \sigma / 2\pi f \varepsilon_0 \quad (2)$$

where f is the frequency of the microwave and ε_0 is the permittivity of the vacuum. Therefore, both the real and imaginary parts of permittivity increased continuously within 0–6 h of ball milling. When the particles reached their plastic deformation limit in ball milling, flaky particles would break. After ball milling for 20 h, ε' and ε'' at 1 GHz decreased to 16.70 and 1.44, respectively. On the one hand, in grains refined by ball milling, the volume fraction of the grain boundary increased [60], indicating the enhancement of electron scattering and a reduction in interparticle eddy currents [61]. On the other hand, SEM images show that particles were broken from flakes to irregular shapes resembling spheres. Contact between particles decreased, thus weakening the interparticle eddy currents.

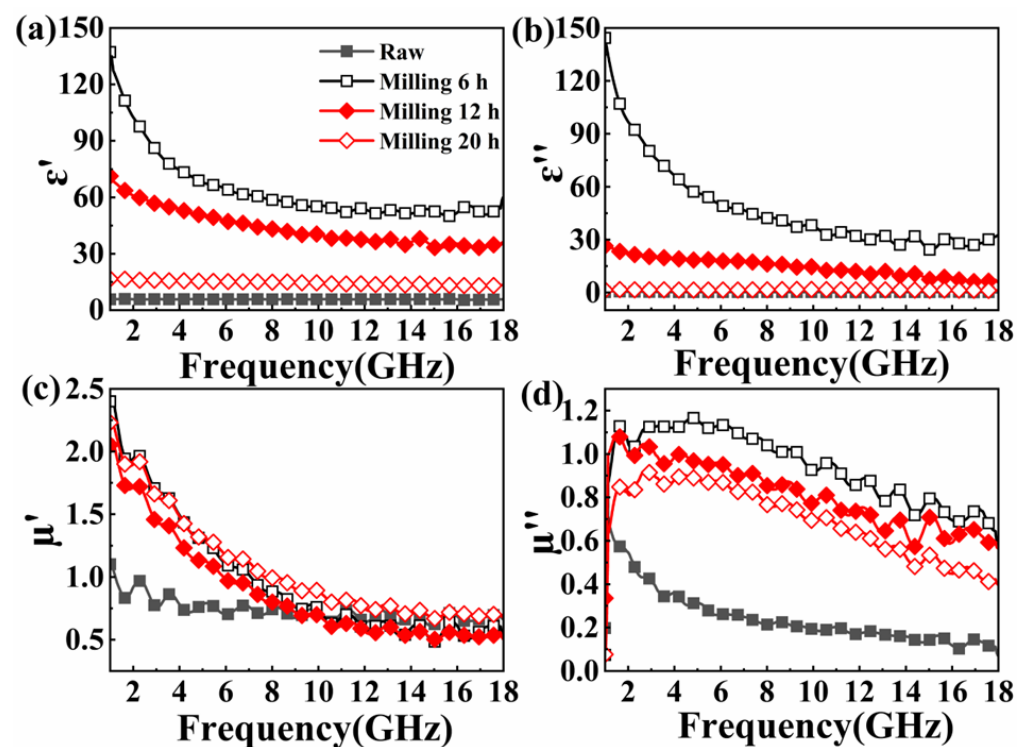


Figure 3. (a,b) Complex permittivity and (c,d) complex permeability of 304 stainless-steel powders after milling for different times.

Figure 3c,d shows the frequency-dependent characteristics of the complex permeability ($\mu_r = \mu' - i\mu''$) of 304 stainless-steel powders in wax over 1.0–18.0 GHz. After ball milling for 6 h, the maximum value of μ' at 1 GHz increased from 1.10 to 2.40, which was attributed to the formation of a martensitic phase and increased shape anisotropy. Orientation and flake shape were expected to break the Snoek limit and obtain high permeability [62]. The μ' at 1 GHz after ball milling for 12 h and 20 h was 2.05 and 2.23, respectively, which was due to the weakening of anisotropy caused by particle cracking; however, the formation of more martensitic phase kept μ' at a high level. The μ'' , which shows the ability to attenuate microwaves, exhibited a typical resonance peak in the microwave band [63]. After ball

milling for 6 h, the maximum value of μ'' increased from 0.15 to 1.20 and showed weak dispersion over 1~18 GHz. With a further increase in ball-milling time, the cracking of particles caused a reduction in the width-to-thickness ratio, the destruction of magnetic domain and a decrease in μ'' .

In order to explore the potential applications of 304 stainless-steel powders as microwave absorbents in long-term service at elevated temperatures, heat treatment in air was carried out at different temperatures and times. The phase, electromagnetic parameters and microwave absorption of the 304 alloy powders during heat treatment were analyzed. Figure 4a shows the XRD pattern of 304 stainless-steel powders after ball milling for 20 h and subsequent heat treatment in air at different temperatures for 1 h. It can be seen that the crystal structure of the 304 alloy powders was stable at temperatures up to 500 °C. The M_s of the powders further increased to 92.29 emu/g after heat treatment, while the H_c increased slightly (see Figure S3 in Supplementary Information). The further increase in M_s may be due to the promotion of martensite transformation by heat treatment, leading to a thermal-deformation-induced ferromagnetism effect. The increase in H_c may be caused by slight oxidation. When heated to 600 °C, an obvious transformation of the martensitic phase back to the austenitic phase occurred, resulting in decrease in M_s to 23.45 emu/g. Figure 4b shows the XRD pattern of 304 stainless-steel powders after heat treatment at 500 °C in air for different times. It can be seen that the crystal structure of 304 stainless-steel powders remained unchanged, and the M_s remained stable at 500 °C for 100 h. The H_c rose slightly and then stabilized at about 190 Oe (see Figure S4 in Supplementary Information). The change in H_c may be due to the synergistic effect of Cr oxidation, carbide precipitation and element segregation [64].

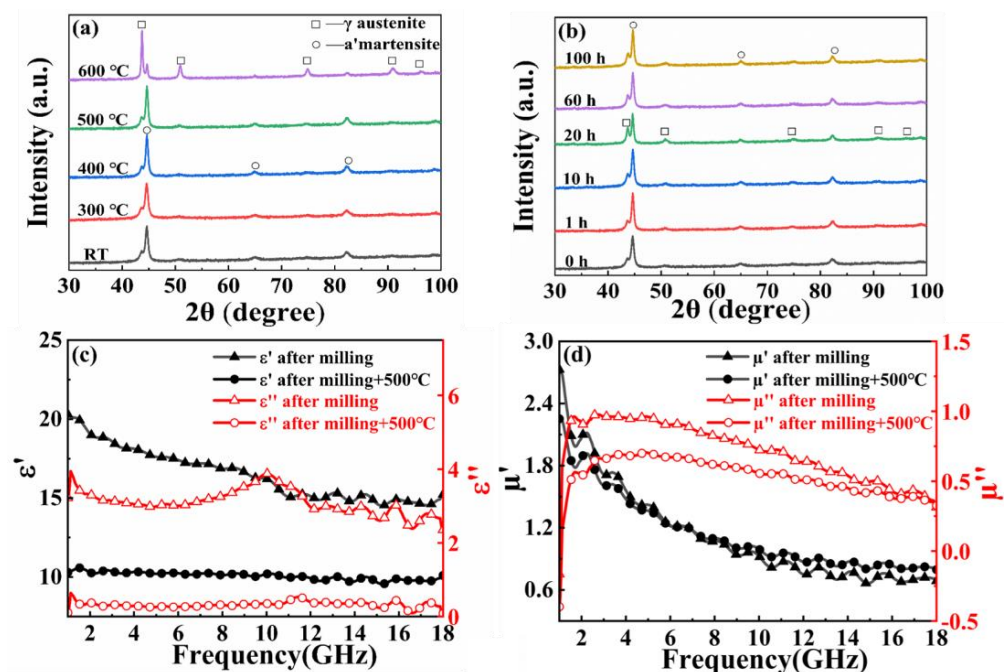


Figure 4. (a,b) XRD pattern of flaky 304 stainless-steel powders after heat treatment in air (a) at different temperatures for 1 h and (b) at 500 °C for different times; (c) complex permittivity and (d) complex permeability of flaky 304 stainless-steel powders before and after heat treatment in air.

The complex permittivity and permeability of flaky 304 stainless-steel powders after heat treatment at 500 °C were further studied. It can be seen from Figure 4c,d that both the real and imaginary parts of the complex permittivity of 304 stainless-steel powders after heat treatment in air dropped significantly. The sharp decrease in permittivity was due to the insulating oxide layer generated on the surface of the powders during heat treatment, thus hindering the formation of conducting networks among flaky powders [65], which

is helpful for reducing eddy-current loss and improving the impedance matching of the material. It can also be seen that the imaginary part of the permeability decreased slightly due to oxidation, indicating a limitation of the alloy strategy for preparing anti-oxidation microwave absorbers.

The microwave absorption properties of 304 stainless-steel powders after ball milling and heat treatment were further investigated. The reflection loss (RL) was simulated using complex permittivity and permeability in accordance with the transmission line theory [66]. Figure 5a shows the RL of 304 stainless-steel powders of various thicknesses after ball milling for 20 h and air heat treatment for 5 h. It is noticed that the material has strong microwave absorption performance at thicknesses greater than 1.5 mm. In Figure 5b, the RL at 2 mm is presented for raw 304 stainless-steel powders and those after ball milling and heat treatment. It can be seen that the absorption by raw powders of microwaves is fairly low. After milling for 20 h, the minimum RL reached -10.6 dB due to a significant transformation of the martensite phase. After further heat treatment in air, an enhancement of absorption can be seen due to the sharp decrease in permittivity and improvement in impedance matching. As a result, the material exhibited a minimum RL of -18.6 dB and an RL below -6 dB over 7–16 GHz. Figure 5b also demonstrates that even after 100 h of heat treatment at 500 °C in air, the microwave absorption of 304 stainless-steel powders remained at a high level, giving a minimum RL of -22 dB and an RL below -6 dB over 8.5–16.5 GHz. Therefore, 304 stainless-steel powders can be used as microwave absorbers for long-term working at temperatures of 500 °C, which enlarges the family of microwave absorbers working in harsh environments.

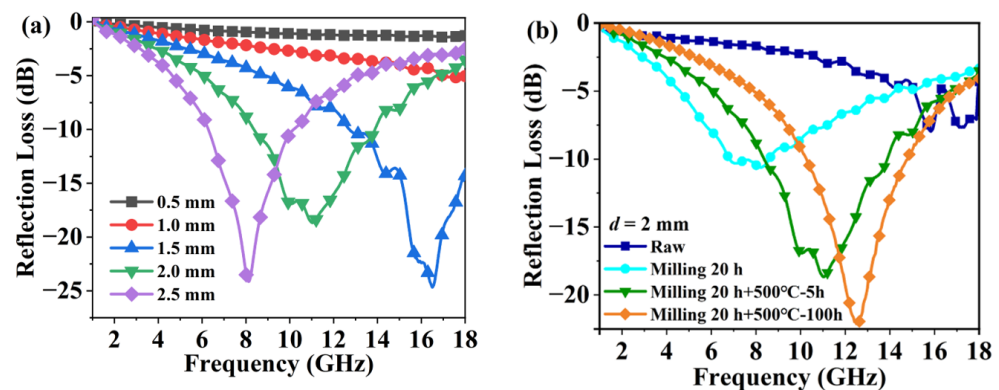


Figure 5. Simulated RL of (a) flaky 304 powders after heat treatment at 500 °C in air and (b) those before and after thermal deformation treatment.

4. Conclusions

In this work, we induced ferromagnetic transformation and shape anisotropy in austenitic 304 stainless-steel powders via deformation to explore their potential as new microwave absorbers working in harsh environments. It was found that the powders changed from spherical to flaky, along with significant transformations from the austenitic to the martensitic phase. The M_s increased sharply from 1.03 to 82.46 emu/g after ball milling, and the μ' at 1 GHz increased obviously from 1.10 to 2.23. After subsequent heat treatment, the M_s further increased to 92.29 emu/g. The martensitic 304 stainless-steel powders were able to tolerate temperatures up to 500 °C with stable phase structure and permeability. After heat treatment in air, the permittivity of the powders was reduced sharply, whereas the permeability remained at a high level, which gave rise to improved impedance matching and microwave absorption. The simulated RL of resultant absorbers in wax reached a minimum of -18.6 dB at 2 mm and showed values below -6 dB over 7–16 GHz. After working at 500 °C in air for 100 h, the RL remained roughly stable, indicating its potential for microwave absorption at elevated temperatures.

Supplementary Materials: The following supporting information can be downloaded at: <https://www.mdpi.com/article/10.3390/magnetochemistry9090208/s1>, Figure S1: SEM images of 304 stainless-steel powders during ball milling; Figure S2: Particle size distribution of 304 stainless-steel powders during ball milling; Figure S3: Hysteresis loop of air after heat treatment at 500 °C and 600 °C for 1 h; Figure S4: The changes of M_s and H_c after heat treatment at 500 °C for different time; Figure S5: Simulated reflection loss after heat treatment at 500 °C for 100 h.

Author Contributions: Conceptualization, Z.C. and W.L.; methodology, B.Y.; software, H.Y.; validation, B.Y., Y.X., Y.H. and M.X.; formal analysis, B.Y. and H.W.; data curation, Z.C.; writing—original draft preparation, B.Y. and Y.X.; writing—review and editing, Z.C. and J.G.; supervision, Z.C. and W.L.; funding acquisition, Z.C. and W.L. All authors have read and agreed to the published version of the manuscript.

Funding: This research was funded by the National Natural Science Foundation of China (Nos. 52071239, 52311530074, 51521001) and the Aeronautical Science Foundation of China (2018ZF65002).

Data Availability Statement: The original contributions presented in the study are included in the article/Supplementary Materials, and further inquiries can be directed to the corresponding authors.

Acknowledgments: The National Innovation and Entrepreneurship Training Program for College Students (202210497012).

Conflicts of Interest: The authors declare no conflict of interest.

References

1. Ding, D.H.; Luo, F.; Zhou, W.C.; Shi, Y.M.; Zhou, L. Research Status and Outlook of High Temperature Radar Absorbing Materials. *J. Inorg. Mater.* **2014**, *29*, 461–469.
2. Wen, B.; Cao, M.; Lu, M.; Cao, W.; Shi, H.; Liu, J.; Wang, X.; Jin, H.; Fang, X.; Wang, W. Reduced graphene oxides: Light-weight and high-efficiency electromagnetic interference shielding at elevated temperatures. *Adv. Mater.* **2014**, *26*, 3484–3489. [[CrossRef](#)]
3. Fu, Z.Y.; Pang, A.M.; Luo, H.; Zhou, K.C.; Yang, H.T. Research progress of ceramic matrix composites for high temperature stealth technology based on multi-scale collaborative design. *J. Mater. Res. Technol.* **2022**, *18*, 2770–2783. [[CrossRef](#)]
4. Qin, F.; Brosseau, C. A review and analysis of microwave absorption in polymer composites filled with carbonaceous particles. *J. Appl. Phys.* **2012**, *111*, 061301. [[CrossRef](#)]
5. Shen, Z.Z.; Chen, J.H.; Li, B.; Li, G.Q.; Zhang, Z.J.; Hou, X.M. Recent progress in SiC nanowires as electromagnetic microwaves absorbing materials. *J. Alloys Compd.* **2020**, *815*, 152388. [[CrossRef](#)]
6. Li, D.; Jia, D.; Yang, Z.; Zhou, Y. Principles, design, structure and properties of ceramics for microwave absorption or transmission at high-temperatures. *Int. Mater. Rev.* **2022**, *67*, 266–297. [[CrossRef](#)]
7. Jia, Z.; Lin, K.; Wu, G.; Xing, H.; Wu, H. Recent progresses of high-temperature microwave-absorbing materials. *Nano* **2018**, *13*, 1830005. [[CrossRef](#)]
8. Sista, K.S.; Dwarapudi, S.; Kumar, D.; Sinha, G.R.; Moon, A.P. Carbonyl iron powders as absorption material for microwave interference shielding: A review. *J. Alloys Compd.* **2021**, *853*, 157251. [[CrossRef](#)]
9. Song, W.L.; Cao, M.S.; Hou, Z.L.; Yuan, J.; Fang, X.Y. High-temperature microwave absorption and evolutionary behavior of multiwalled carbon nanotube nanocomposite. *Scr. Mater.* **2009**, *61*, 201–204. [[CrossRef](#)]
10. Li, J.S.; Huang, H.; Zhou, Y.J.; Zhang, C.Y.; Li, Z.T. Research progress of graphene-based microwave absorbing materials in the last decade. *J. Mater. Res.* **2017**, *32*, 1213–1230. [[CrossRef](#)]
11. Wang, F.; Long, C.; Wu, T.L.; Li, W.; Chen, Z.H.; Xia, F.J.; Wu, J.S.; Guan, J.G. Enhancement of low-frequency magnetic permeability and absorption by texturing flaky carbonyl iron particles. *J. Alloys Compd.* **2020**, *823*, 153827. [[CrossRef](#)]
12. Wei, H.Y.; Zhang, Z.P.; Hussain, G.; Zhou, L.S.; Li, Q.; Ostrikov, K. Techniques to enhance magnetic permeability in microwave absorbing materials. *Appl. Mater. Today* **2020**, *19*, 100596. [[CrossRef](#)]
13. Saber, M.; Kotan, H.; Koch, C.C.; Scattergood, R.O. Thermal stability of nanocrystalline Fe-Cr alloys with Zr additions. *Mater. Sci. Eng. A-Struct. Mater. Prop. Microstruct. Process.* **2012**, *556*, 664–670. [[CrossRef](#)]
14. Lezaic, M.; Mavropoulos, P.; Blugel, S. First-principles prediction of high Curie temperature for ferromagnetic bcc-Co and bcc-FeCo alloys and its relevance to tunneling magnetoresistance. *Appl. Phys. Lett.* **2007**, *90*, 082504. [[CrossRef](#)]
15. Yuan, D.C.; Chen, Z.Y.; Cai, C.W.; Yang, B.L.; Wang, Y.J.; Chen, Z.H. Microstructures, absorption and adhesion evolution of FeCoCr/silicone resin coatings at elevated temperature. *Front. Mater.* **2023**, *10*, 1168418. [[CrossRef](#)]
16. Fu, Z.W.; Chen, Z.H.; Wang, R.; Xiao, H.Y.; Wang, J.; Yang, H.; Shi, Y.T.; Li, W.; Guan, J.G. Deformation-Thermal Co-Induced Ferromagnetism of Austenite Nanocrystalline FeCoCr Powders for Strong Microwave Absorption. *Nanomaterials* **2022**, *12*, 2263. [[CrossRef](#)]
17. Gómez-Polo, C.; Pérez-Landazabal, J.; Recarte, V.; Campo, J.; Marín, P.; López, M.; Hernando, A.; Vázquez, M. High-temperature magnetic behavior of FeCo-based nanocrystalline alloys. *Phys. Rev. B* **2002**, *66*, 012401. [[CrossRef](#)]

18. Yin, C.L.; Fan, J.M.; Bai, L.Y.; Ding, F.; Yuan, F.L. Microwave absorption and antioxidation properties of flaky carbonyl iron passivated with carbon dioxide. *J. Magn. Magn. Mater.* **2013**, *340*, 65–69. [[CrossRef](#)]
19. Zhou, Y.Y.; Xie, H.; Zhou, W.C.; Ren, Z.W. Enhanced antioxidation and microwave absorbing properties of SiO₂-coated flaky carbonyl iron particles. *J. Magn. Magn. Mater.* **2018**, *446*, 143–149. [[CrossRef](#)]
20. Xu, Z.G.; Du, J.H.; Wang, J.; Chen, Z.H.; Lie, W.J.; Wang, C.B.; Shen, Q. A comparative study on the microwave absorption properties of core-single-shell, core-double-shell and yolk-shell CIP/ceramic composite microparticles. *J. Magn. Magn. Mater.* **2022**, *547*, 168959. [[CrossRef](#)]
21. Abshinova, M.A.; Kazantseva, N.E.; Saha, P.; Sapurina, I.; Kovarova, J.; Stejskal, J. The enhancement of the oxidation resistance of carbonyl iron by polyaniline coating and consequent changes in electromagnetic properties. *Polym. Degrad. Stab.* **2008**, *93*, 1826–1831. [[CrossRef](#)]
22. Jia, K.; Xu, M.Z.; Zhao, R.; Liu, X.B. Chemically bonded iron carbonyl for magnetic composites based on phthalonitrile polymers. *Polym. Int.* **2011**, *60*, 414–421. [[CrossRef](#)]
23. Yan, L.; Wang, J.; Han, X.; Ren, Y.; Liu, Q.; Li, F. Enhanced microwave absorption of Fe nanoflakes after coating with SiO₂ nanoshell. *Nanotechnology* **2010**, *21*, 095708. [[CrossRef](#)]
24. Guo, Y.; Jian, X.; Zhang, L.; Mu, C.; Yin, L.; Xie, J.; Mahmood, N.; Dou, S.; Che, R.; Deng, L. Plasma-induced FeSiAl@ Al₂O₃@ SiO₂ core-shell structure for exceptional microwave absorption and anti-oxidation at high temperature. *Chem. Eng. J.* **2020**, *384*, 123371. [[CrossRef](#)]
25. Zhao, D.; Luo, F.; Zhou, W.C.; Zhu, D.M. Complex Permittivity and Microwave-Absorbing Properties of Fe/Al₂O₃ Coatings by Air Plasma Spraying Technique. *Int. J. Appl. Ceram. Technol.* **2013**, *10*, E88–E97. [[CrossRef](#)]
26. Wang, H.Y.; Zhu, D.M.; Zhou, W.C.; Luo, F. Enhanced microwave absorbing properties and heat resistance of carbonyl iron by electroless plating Co. *J. Magn. Magn. Mater.* **2015**, *393*, 445–451. [[CrossRef](#)]
27. Jia, S.; Luo, F.; Qing, Y.C.; Zhou, W.C.; Zhu, D.M. Electroless plating preparation and microwave electromagnetic properties of Ni-coated carbonyl iron particle/epoxy coatings. *Phys. B-Condens. Matter* **2010**, *405*, 3611–3615. [[CrossRef](#)]
28. Chen, Z.H.; Hwang, S.H.; Zeng, X.B.; Roh, J.; Jang, J.; Ungar, G. SAXS characterization of polymer-embedded hollow nanoparticles and of their shell porosity. *J. Appl. Crystallogr.* **2013**, *46*, 1654–1664. [[CrossRef](#)]
29. Chen, Z.H.; Kim, C.; Zeng, X.B.; Hwang, S.H.; Jang, J.; Ungar, G. Characterizing Size and Porosity of Hollow Nanoparticles: SAXS, SANS, TEM, DLS, and Adsorption Isotherms Compared. *Langmuir* **2012**, *28*, 15350–15361. [[CrossRef](#)]
30. May, J.E.; Galerie, A.; Busquim, T.P.; Kuri, S.E. High temperature oxidation behavior of FeCo-based nanocrystalline alloys. *Mater. Corros. -Werkst. Und Korros.* **2007**, *58*, 87–91. [[CrossRef](#)]
31. Gupta, R.K.; Raman, R.K.S.; Koch, C.C. Fabrication and oxidation resistance of nanocrystalline Fe₁₀Cr alloy. *J. Mater. Sci.* **2010**, *45*, 4884–4888. [[CrossRef](#)]
32. Cao, G.J.; Geng, L.; Zheng, Z.Z.; Naka, M. The oxidation of nanocrystalline Ni₃Al fabricated by mechanical alloying and spark plasma sintering. *Intermetallics* **2007**, *15*, 1672–1677. [[CrossRef](#)]
33. Nova, K.; Novak, P.; Prusa, F.; Kopecek, J.; Cech, J. Synthesis of Intermetallics in Fe-Al-Si System by Mechanical Alloying. *Metals* **2019**, *9*, 20. [[CrossRef](#)]
34. Lo, K.H.; Shek, C.H.; Lai, J.K.L. Recent developments in stainless steels. *Mater. Sci. Eng. R-Rep.* **2009**, *65*, 39–104. [[CrossRef](#)]
35. Yang, R.B.; Liang, W.F.; Lou, C.W.; Lin, J.H. Electromagnetic and microwave absorption properties of magnetic stainless steel powder in 2–18 GHz. *J. Appl. Phys.* **2012**, *111*, 07A338. [[CrossRef](#)]
36. Shanmugam, K.; Lakshminarayanan, A.K.; Balasubramanian, V. Tensile and Impact Properties of Shielded Metal Arc Welded AISI 409M Ferritic Stainless Steel Joints. *J. Mater. Sci. Technol.* **2009**, *25*, 181–186.
37. Sabioni, A.C.S.; Huntz, A.-M.; Luz, E.C.d.; Mantel, M.; Haut, C. Comparative study of high temperature oxidation behaviour in AISI 304 and AISI 439 stainless steels. *Mater. Res.* **2003**, *6*, 179–185. [[CrossRef](#)]
38. Engin, C.; Sandoval, L.; Urbassek, H.M. Characterization of Fe potentials with respect to the stability of the bcc and fcc phase. *Model. Simul. Mater. Sci. Eng.* **2008**, *16*, 035005. [[CrossRef](#)]
39. Soleimani, M.; Kalhor, A.; Mirzadeh, H. Transformation-induced plasticity (TRIP) in advanced steels: A review. *Mater. Sci. Eng. A-Struct. Mater. Prop. Microstruct. Process.* **2020**, *795*, 140023. [[CrossRef](#)]
40. De, A.K.; Murdock, D.C.; Mataya, M.C.; Speer, J.G.; Matlock, D.K. Quantitative measurement of deformation-induced martensite in 304 stainless steel by X-ray diffraction. *Scr. Mater.* **2004**, *50*, 1445–1449. [[CrossRef](#)]
41. Murr, L.; Staudhammer, K.; Hecker, S. Effects of strain state and strain rate on deformation-induced transformation in 304 stainless steel: Part II. Microstructural study. *Metall. Trans. A* **1982**, *13*, 627–635. [[CrossRef](#)]
42. Huang, H.; Ding, J.; McCormick, P. Microstructural evolution of 304 stainless steel during mechanical milling. *Mater. Sci. Eng. A* **1996**, *216*, 178–184. [[CrossRef](#)]
43. Lee, E.-S.; Ahn, S. Solidification progress and heat transfer analysis of gas-atomized alloy droplets during spray forming. *Acta Metall. Mater.* **1994**, *42*, 3231–3243. [[CrossRef](#)]
44. Suo, Q.T.; Xu, B.C.; Wang, J.J.; Huang, B.Y. Effect of High Energy Ball Milling on Electromagnetic Properties of FeNi Absorbing Materials. In Proceedings of the 2nd International Conference on Advances in Materials, Machinery, Electronics (AMME), Xi'an, China, 20–21 January 2018.
45. Shashanka, R.; Chaira, D. Development of nano-structured duplex and ferritic stainless steels by pulverisette planetary milling followed by pressureless sintering. *Mater. Charact.* **2015**, *99*, 220–229.

46. Han, F.; Lin, G.Y.; Li, Q.; Long, R.F.; Peng, D.S.; Zhou, Q. Influence of different deformation on microstructure and properties of 304 austenitic stainless steel. *Adv. Mater. Res.* **2012**, *500*, 690–695. [[CrossRef](#)]
47. Zhang, D.L. Processing of advanced materials using high-energy mechanical milling. *Prog. Mater. Sci.* **2004**, *49*, 537–560. [[CrossRef](#)]
48. Esmailzadeh, R.; Salimi, M.; Zamani, C.; Hadian, A.M.; Hadian, A. Effects of milling time and temperature on phase evolution of AISI(316) stainless steel powder and subsequent sintering. *J. Alloys Compd.* **2018**, *766*, 341–348. [[CrossRef](#)]
49. Pan, C.; Su, Y.J.; Chu, W.Y.; Li, Z.B.; Liang, D.T.; Qiao, L.J. Hydrogen embrittlement of weld metal of austenitic stainless steels. *Corros. Sci.* **2002**, *44*, 1983–1993. [[CrossRef](#)]
50. Sohrabi, M.J.; Naghizadeh, M.; Mirzadeh, H. Deformation-induced martensite in austenitic stainless steels: A review. *Arch. Civ. Mech. Eng.* **2020**, *20*, 124. [[CrossRef](#)]
51. Ryoo, D.Y.; Kang, N.; Kang, C.Y. Effect of Ni content on the tensile properties and strain-induced martensite transformation for 304 stainless steel. *Mater. Sci. Eng. A-Struct. Mater. Prop. Microstruct. Process.* **2011**, *528*, 2277–2281. [[CrossRef](#)]
52. Menendez, E.; Sort, J.; Liedke, M.O.; Fassbender, J.; Surinach, S.; Baro, M.D.; Nogues, J. Controlled generation of ferromagnetic martensite from paramagnetic austenite in AISI 316L austenitic stainless steel. *J. Mater. Res.* **2009**, *24*, 565–573. [[CrossRef](#)]
53. Delogu, F. A few details of the austenite to martensite phase transformation in 304 stainless steel powders under mechanical processing. *Acta Mater.* **2011**, *59*, 2069–2074. [[CrossRef](#)]
54. Oleszak, D.; Grabias, A.; Pekala, M.; Swiderska-Sroda, A.; Kulik, T. Evolution of structure in austenitic steel powders during ball milling and subsequent sintering. *J. Alloys Compd.* **2007**, *434*, 340–343. [[CrossRef](#)]
55. Zhang, B.; Duan, Y.P.; Cui, Y.L.; Ma, G.J.; Wang, T.M.; Dong, X.L. A new mechanism for improving electromagnetic properties based on tunable crystallographic structures of FeCoNiSi_xAl_{0.4} high entropy alloy powders. *Rsc Adv.* **2018**, *8*, 14936–14946. [[CrossRef](#)]
56. Zhang, B.; Duan, Y.P.; Wen, X.; Ma, G.J.; Wang, T.M.; Dong, X.L.; Zhang, H.F.; Jia, N.; Zeng, Y.S. FeCoNiSi_xAl_{0.4} high entropy alloy powders with dual-phase microstructure: Improving microwave absorbing properties via controlling phase transition. *J. Alloys Compd.* **2019**, *790*, 179–188. [[CrossRef](#)]
57. Ding, J.; Huang, H.; McCormick, P.; Street, R. Magnetic properties of martensite-austenite mixtures in mechanically milled 304 stainless steel. *J. Magn. Magn. Mater.* **1995**, *139*, 109–114. [[CrossRef](#)]
58. Zhou, Y.Y.; Ma, L.Y.; Li, R.; Chen, D.; Lu, Y.Y.; Cheng, Y.Y.; Luo, X.X.; Xie, H.; Zhou, W.C. Enhanced heat-resistance property of aluminum-coated carbonyl iron particles as microwave absorption materials. *J. Magn. Magn. Mater.* **2021**, *524*, 167681. [[CrossRef](#)]
59. Huang, C.; Dong, Q.; Yin, X.; Zhang, R.Z.; Zhang, Y.J.; Yang, D.A. Antioxidation and electromagnetic properties of Co-coated hollow carbonyl iron particles by electroless plating method. *J. Mater. Sci. Mater. Electron.* **2017**, *28*, 5037–5043. [[CrossRef](#)]
60. Song, H.; Guo, S.; Hu, Z. A coherent polycrystal model for the inverse Hall-Petch relation in nanocrystalline materials. *Nanostructured Mater.* **1999**, *11*, 203–210. [[CrossRef](#)]
61. Ren, X.; Corcolle, R.; Daniel, L. A homogenization technique to calculate eddy current losses in soft magnetic composites using a complex magnetic permeability. *IEEE Trans. Magn.* **2016**, *52*, 1–9. [[CrossRef](#)]
62. Yang, W.Y.; Zhang, Y.F.; Qiao, G.Y.; Lai, Y.F.; Liu, S.Q.; Wang, C.S.; Han, J.Z.; Du, H.L.; Zhang, Y.; Yang, Y.C.; et al. Tunable magnetic and microwave absorption properties of Sm_{1.5}Y_{0.5}Fe_{17-x}Si_x and their composites. *Acta Mater.* **2018**, *145*, 331–336. [[CrossRef](#)]
63. Jia, Z.; Zhu, Z.H.; Zeng, C.C.; Zhao, H.; Yuan, Z.F. The effect of yttrium on the microwave absorbing properties of Fe₇₈Si₁₃B₉ alloy powders. *Chem. Eng. J.* **2020**, *398*, 124444. [[CrossRef](#)]
64. Gauzzi, F.; Montanari, R.; Principi, G.; Tata, M.E. AISI 304 steel: Anomalous evolution of martensitic phase following heat treatments at 400 degrees C. *Mater. Sci. Eng. A-Struct. Mater. Prop. Microstruct. Process.* **2006**, *438*, 202–206. [[CrossRef](#)]
65. Li, M.; Yin, X.W.; Zheng, G.P.; Chen, M.; Tao, M.J.; Cheng, L.F.; Zhang, L.T. High-temperature dielectric and microwave absorption properties of Si₃N₄-SiC/SiO₂ composite ceramics. *J. Mater. Sci.* **2015**, *50*, 1478–1487. [[CrossRef](#)]
66. Yu, M.; Yang, P.A.; Fu, J.; Liu, S.Z. Flower-like carbonyl iron powder modified by nanoflakes: Preparation and microwave absorption properties. *Appl. Phys. Lett.* **2015**, *106*, 161904. [[CrossRef](#)]

Disclaimer/Publisher's Note: The statements, opinions and data contained in all publications are solely those of the individual author(s) and contributor(s) and not of MDPI and/or the editor(s). MDPI and/or the editor(s) disclaim responsibility for any injury to people or property resulting from any ideas, methods, instructions or products referred to in the content.